Multimedia Tools and Applications (2024) 83:2323–2347
https://doi.org/10.1007/s11042-023-15242-y

# A structure and texture revealing retinex model for low-light image enhancement

**Xuesong Li[1] · Qilei Li[2] · Marco Anisetti[3] · Gwanggil Jeon[4] · Mingliang Gao[1]**

Received: 23 June 2022 / Revised: 30 January 2023 / Accepted: 30 March 2023 /
Published online: 13 May 2023


**Abstract**
Low-light image enhancement is a crucial yet challenging task in computer vision and multimedia applications. Retinex-based approaches have been continuously explored in this domain. However, the Retinex decomposition is an ill-posed problem, as the proper constraints of illumination and reflectance should be considered to regularize the solution space. Aiming at a faithful enhancement, we develop a Structure and Texture Revealing Retinex (STR$^2$) model to accurately estimate the illumination and reflectance components. The proposed STR$^2$ model utilizes an exponential relative total variation method to draw structure and texture maps by analyzing the difference in gradient distribution between the illumination and reflectance components. The resulting structure and texture maps are used to regularize the illumination and reflectance components. With a tailored alternating optimization algorithm, the STR$^2$ model can jointly update the illumination and reflectance efficiently to produce a faithful enhanced image. Experimental results on several public datasets verify the effectiveness of the proposed model in low-light image enhancement.

**Keywords** Low-light image enhancement · Retinex decomposition · Illumination adjustment · Structure estimation · Texture estimation

## 1 Introduction

The images acquired in low-light scenarios, *e.g.*, in the darkness or nighttime, suffer from the absence of pleasing visual aesthetics and enormous amount of mingled noise, low contrast and color distortions. The low-light images hider the performance of subsequent

✉ Mingliang Gao
mlgao@sdut.edu.cn

1 School of Electrical and Electronic Engineering, Shandong University of Technology, Zibo, 255000, China

2 School of Electronic Engineering and Computer Science, Queen Mary University of London, London, United Kingdom, E1 4NS

3 Department of Computer Science, University of Milan, Milano, Italy, 20133

4 Department of Embedded Systems Engineering, Incheon National University, Incheon, South Korea, 22012

computer vision applications. Besides, with the boom and prevalence of portable imaging devices, the demand for high-quality images with clear details and satisfied brightness becomes extremely imperative. Hence, it is crucial to develop an effective and robust algorithm for low-light image enhancement under various realistic scenes.

The existing enhancement methods can be divided into three categories, namely histogram equalization-based methods [1, 21], Retinex decomposition-based methods [32, 47], and deep learning-based methods [40, 53]. The histogram equalization (HE) methods are global illumination-adjusted methods that enhance the images by stretching the entire dynamic range of the image. However, these methods are lame in adjusting the local information. Developed by Land and McCann [29], Retinex theory decomposes the image into illumination and reflectance components and enhances them separately. It builds a robust and flexible baseline framework for low-light image enhancement [8]. The variational Retinex approaches are used to enforce the continuous on reflectance layer and piece-wise smooth on illumination layer [10, 28]. Recently, a robust Retinex model has been proposed by Li et al. [34]. However, they simply assumed that the illumination component is sufficient enough that no further processing is required, which results in observable noise appearing in the reflectance component when this assumption is not met. Besides, deep learning-based methods have also been widely studied. Since the pioneering work of Bychkovsky et al. [3], more efforts have been focused on investigating learning-based approaches. The data-driven low-light image enhancement methods utilize either the traditional machine learning techniques such as LTR [62], or deep neural networks DeepExposure [64], DeepBL [14], KinD [67], and SID [6]. However, learning-based methods requires a huge amount of training samples for modeling the mapping, which is not quite easy to satisfy in many real-world applications.

In this paper, we conduct an effective method to accomplish the structure and texture estimation during the Retinex decomposition. The proposed model is based on two highly correlated hypotheses, *i.e.*, the illumination component should be piece-wise smooth, while the reflectance component should contain as much detail as possible. To this aim, we build a Structure and Texture Revealing Retinex (STR$^2$) model. This model can achieve remarkable achievement in low-light image enhancement. The overall architecture of the proposed model is shown in Fig. 1. In a nutshell, the contributions of this paper are as follows:

1. We develop a Structure and Texture Revealing Retinex (STR$^2$) model which can accurately estimate the illumination and reflectance components by building weight matrices for structures and textures.
2. The proposed STR$^2$ model utilizes an exponential relative total variation method to draw structure and texture maps by analyzing the difference in gradient distribution between the illumination and reflectance components.
3. Experiments on several challenging benchmarks prove the effectiveness of the proposed STR$^2$ model in Retinex decomposition and low-light image enhancement.

The organization of this paper is as follows: In Section 2, the methods of low-light image enhancement are reviewed. Section 3 introduces the theoretical background, including the basic Retinex theory and structure-texture decomposition. In Section 4, the proposed approach is detailed. Experimental results are demonstrated in Section 5. The work is concluded in Section 6.

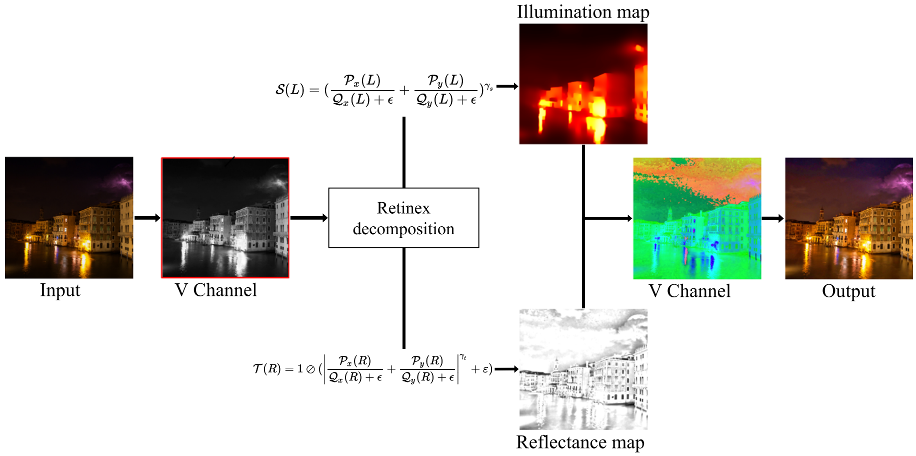


**Fig. 1** The framework of the proposed STR$^2$ model. Given the input low-light RGB image, it is first converted into HSV space. The $V$ channel is normalized and decomposed into illumination and reflectance components. Then, these two components are adjusted by calculating the structure and texture weight matrix, respectively. The adjusted illumination component and reflectance component are integrated and the enhanced HSV image is transformed into the RGB space to obtain the final output result

## 2 Related work

In this section, the methods for low-light image enhancement are briefly reviewed. These methods can be generally divided into three categories, namely histogram equalization-based [45], Retinex decomposition-based [32], and learning-based models [39].

**Histogram equalization (HE)-based methods** improve the visibility of low-light images by flattening the histogram via stretching the corresponding dynamic range of the intensity [51]. HE-based methods can be further classified into global HE-based methods and local HE-based methods. As for global HE-based methods [25, 65], the total histogram is utilized to enhance the dynamic range of low-light image and improve the brightness. However, these methods may cause significant detail information lost and noise amplified during enhanced processing. Instead of manipulating the total histogram, the local HE-based methods [38, 52, 54] enhance the local region which is divided from the entire histogram. The local HE-based methods perform better on low-frequency information processing than the global counterparts, but the computational complexity is significantly increased. In order to degrade the complexity of computation, some researchers proposed parametric HE-based methods [36, 37]. Although these methods are particularly effective for contrast or dynamic range enhancement, the enhanced image often exhibits unnatural details.

**Retinex decomposition-based methods** enhance low-light images by image decomposition. These methods decompose the images into two components, namely reflectance and illumination components. Then, these two components are further processed to obtain enhanced results. The single-scaled Retinex (SSR) [23] method and multi-scaled Retinex (MSR) [24] method are the pioneering works in this field. Subsequent methods consider both the illumination and reflectance layers to improve the performance [34, 49]. However, it's inherently an ill-posed problem to estimate illumination and reflectance components from a single image. In order to make the problem trackable, some attempts to transform the illumination or reflectance decomposition into a statistical reasoning problem and seek the most suitable solutions by proposing different priors for illumination and reflectance and defining variational optimization [10, 46]. Kimmel et al. [28] proposed a variation method to estimate the illumination component solely and postulated that it should be varied smoothly. Subsequently, a total variational (TV) Retinex decomposition model considering both the reflectance and illumination components was proposed [43]. However, this approach can result in over-smoothing in the reflectance map owning to the by-product of logarithmic transformations. To address this problem, Fu et al. [12] proposed a linear domain model to improve the representation of the prior information. Recently, some methods revisited the local variance model to draw structure and texture maps [4]. Proposed by Xu et al. [61], the STAR utilized the exponential local variance constraints to reveal the structure and texture in illumination and reflectance maps. These methods perform well in stretching image contrast and noise removal. However, due to the poor adaptability of the method and related prior, they may produce undesirable results when applied to large-scale datasets [39].

**Learning-based methods** model the feature maps from the high visual quality images to enhance the low-light images. Lore et al. [40] first enhanced the low-light images by stacking sparse auto-encoders. Subsequently, different networks and diversified losses were proposed [7, 27, 66]. In addition, Retinex theory joins up with deep learning methods for low-light enhancement. Wei et al. [57] proposed the Retinex-Net with two subnets. First, a Decom-Net decomposes an image into reflectance and illumination components. Then, the estimated illumination is enhanced by Enhance-Net. Besides, adversarial learning was introduced to obtain visual attributes beyond traditional metrics [22, 26]. Jiang et al. [22] proposed an EnlightenGAN to get rid of the construction of pairwise datasets. Although the deep learning-based approaches have achieved remarkable achievements in the domain of low-light image enhancement, the enormous computational burden in practical application and the complex structure of the model limit their popularity on mobile devices. Moreover, the learning-based methods rely heavily on plenty of high-quality images.

## 3 Theoretical background

### 3.1 Retinex theory

The Retinex theory [2] postulates that the input low-light image $I \in \mathbb{R}^{n\times m}$ can be represented as the product of the illumination $L \in \mathbb{R}^{n\times m}$ and the reflectance $R \in \mathbb{R}^{n\times m}$:

$$I = L \odot R, \tag{1}$$

The symbol $\odot$ means element-wise multiplication. The decomposed components can be converted back by estimating them alternatively by

$$L = I \oslash R, \quad R = I \oslash L, \tag{2}$$

where $\oslash$ represents the element-wise division.

Retinex theory introduces a valuable derivative property [29], *i.e.*, variation of the reflectance component usually results in the larger derivative value in the image, while the smaller derivative value is due to the smooth distribution of the illumination. According to the properties of the image in the gradient field, the prior variational Retinex methods generally utilize a variational objective function to estimate the illumination and reflectance components. The objective function is formulated as

$$\min_{L,R} \|I - L \odot R\|_F^2 + \mathcal{N}_1(L) + \mathcal{N}_2(R), \tag{3}$$

where $\mathcal{N}_1$ and $\mathcal{N}_2$ are regularization terms for illumination $L$ and reflectance $R$, respectively.

### 3.2 Structure and texture preserving

Since the Retinex decomposition is an ill-posed problem, constraints, *i.e.,* $\mathcal{N}_1$ and $\mathcal{N}_2$ in (3), are imposed to estimate the illumination and reflectance maps with specific information revealing [35, 43]. The illumination is assumed to be piece-wise smooth due to the shape of objects. The large-scale variations, *e.g.*, structure of the object, are captured in the illumination layer, which results in the small gradient of the layer. Meanwhile, the reflectance layer is assumed to be piece-wise continuous due to the intrinsic property of the object. The small-scale variations, *e.g.*, texture, are captured in the reflectance layer, which results in the large gradient of the layer. To this aim, some researchers imposed structure preserving constrain to estimate the illumination component and exponential decay structure-preserving constrain to estimate the reflectance component [4].

## 4 Methodology

### 4.1 ERTV-based constraints for decomposed components

As mentioned above, the illumination and reflectance components should be estimated with appropriate constraints. To this end, we put forward diverse exponential relative total variation methods to conduct different constraints for illumination and reflectance components.

The previous relative total variation method mainly considers the relationship between the central pixel and the neighbor pixels by using the window-based total variation and inherent variation [59]. The windowed total variation $\mathcal{P}_x$ and $\mathcal{P}_y$ of the central pixel in vertical and horizontal directions are formulated as

$$\mathcal{P}_{x/y} = \sum_{q \in R(p)} G_\sigma * \left|\nabla_{x/y} I_q\right|. \tag{4}$$

And the windowed inherent variation $\mathcal{Q}_x$ and $\mathcal{Q}_y$ are defined as

$$\mathcal{Q}_{x/y} = \left|\sum_{q \in R(p)} G_\sigma * \nabla_{x/y} I_q\right|. \tag{5}$$

Where $I$ is the input image, $\nabla_{x/y}$ is partial derivative in the horizontal or vertical direction and $G_\sigma$ is a Gaussian kernel with window size $\sigma = 3$. The symbol $*$ is a convolutional operator. $R(p)$ is a rectangular region centered on the pixel $p$ and the pixel $q$ belongs to $R(p)$.

However, the previous relative total variation mainly focuses on the relatively small variance suppression to extract the structure, which is easily affected by texture. To address this issue, diverse exponents are introduced to conduct novel constraints. The proposed structure constraint is to enforce spatial smoothness on the illumination layer while preserving the main structure. And the proposed texture constraint is to enforce the reflectance component to be piece-wise continuous. The formulation of the structure constrains is given as

$$\mathcal{S}(I) = (\frac{\mathcal{P}_x(I)}{\mathcal{Q}_x(I)+\epsilon} + \frac{\mathcal{P}_y(I)}{\mathcal{Q}_y(I)+\epsilon})^{\gamma_s}. \tag{6}$$

Since the previous relative total variation method is used as the structure-preserving constrain, the texture constrain is proposed by exponential decay and formulated as

$$\mathcal{T}(I) = 1 \oslash (\left|\frac{\mathcal{P}_x(I)}{\mathcal{Q}_x(I)+\epsilon} + \frac{\mathcal{P}_y(I)}{\mathcal{Q}_y(I)+\epsilon}\right|^{\gamma_t} + \varepsilon). \tag{7}$$

Where $\epsilon$=0.001 and $\varepsilon$=0.005. $\gamma_s$ and $\gamma_t$ are the structure and texture perception coefficients.

### 4.2 STR$^2$ model

The proposed Structure and Texture Revealing Retinex (STR$^2$) model is formulated as,

$$\arg\min_{L,R} \|I - L \odot R\|_F^2 + \alpha \|\mathcal{S} \odot \nabla L\|_F^2 + \beta \|\mathcal{T} \odot \nabla R\|_F^2 + \lambda \|L - B\|_F^2, \tag{8}$$

where $\alpha$, $\beta$ and $\lambda$ are the parameters that control the importance of different terms in object function. In this paper, given the input low-light RGB image, it is first converted into HSV space. Then, the $V$ channel is normalized and decomposed into illumination and reflectance components. Thus, the observed image $I$ is regarded as $V$ channel. The role of each term is interpreted as follows:

- $\|I - L \odot R\|_F^2$ constraints the fidelity between the observed image $I$ and the reconstructed image $L \odot R$;
- $\|\mathcal{S} \odot \nabla L\|_F^2$ and $\|\mathcal{T} \odot \nabla R\|_F^2$ are regularization terms to compute the weight of structure and texture;
- $\|L - B\|_F^2$ minimizes the distance between estimated illumination $L$ and the initial illumination $B$.

The second and third regularization terms in (8) are meant to extract the structure and texture maps by distinguishing the difference in the distribution of gradients between the illumination and reflectance components. The flowchart to demonstrate the principle of low-light image enhancement is shown in Fig. 2.

The smooth illumination results in the smaller gradient [29], while the larger gradient is due to the piece-wise continuous reflectance. The formulations of the second and third terms in the (8) are denoted as

$$\|\mathcal{S} \odot \nabla L\|_F^2 = s_x \|\nabla_x L\|_F^2 + s_y \left\|\nabla_y L\right\|_F^2, \tag{9}$$

$$\|\mathcal{T} \odot \nabla R\|_F^2 = t_x \|\nabla_x R\|_F^2 + t_y \left\|\nabla_y R\right\|_F^2, \tag{10}$$

where

$$s_{x/y} = (\frac{\mathcal{P}_{x/y}(L)}{\mathcal{Q}_{x/y}(L)+\epsilon})^{\gamma_s}, \tag{11}$$

$$t_{x/y} = 1 \oslash (\left|\frac{\mathcal{P}_{x/y}(R)}{\mathcal{Q}_{x/y}(R)+\epsilon}\right|^{\gamma_t} + \varepsilon). \tag{12}$$

The extracted structure and texture maps by the proposed model are depicted in Fig. 3. It can correctly reflect the general outline of the object (*e.g.*, the horn and beard), and the details (*e.g.*, the spot and the eyes) can be revealed.

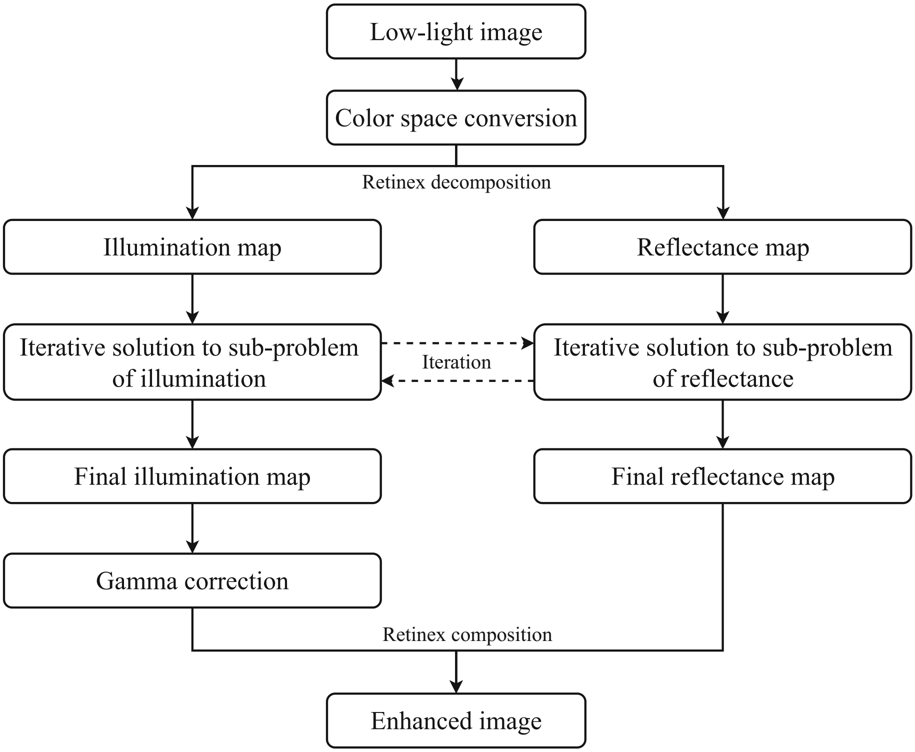


**Fig. 2** The flowchart of the STR$^2$ for low-light image enhancement

### 4.3 Optimization algorithm

$L_k$ and $R_k$ are the illumination and reflectance components at the $k$-th iteration ($k$ =0, 1, 2,..., $K$), respectively. $K$ is the maximum number of iterations. Two separated sub-problems are iteratively cycled through. The solutions to the sub-problems are presented as follows.

**1)** ***L* Sub-problem** Neglecting the terms unrelated to $L$ and initializing $L_0 = I$, the solution to update $(k+1)$-th iteration $L_{k+1}$ is formulated as

$$L_{k+1} = \arg\min_{L_k} \|I - L_k \odot R_k\|_F^2$$
$$+\alpha(s_x \|\nabla_x L_k\|_F^2 + s_y \left\|\nabla_y L_k\right\|_F^2) + \lambda \|L_k - B\|_F^2. \tag{13}$$

To solve (13), the loss function to the matrix notation form is rewritten as

$$L_{k+1} = (L_k \odot R_k - I)^T (L_k \odot R_k - I)$$
$$+\alpha(L_k^T D_x^T S_x D_x L_k + L_k^T D_y^T S_y D_y L_k) + \lambda(L_k - B)^T (L_k - B), \tag{14}$$

where $D_x$ and $D_y$ are the Toeplitz matrices in horizontal and vertical directions. $S_x = diag(s_x)$ and $S_y = diag(s_y)$. Then, the solution to (13) is:

$$L_{k+1} = \frac{R_k^T I + \lambda B}{R_k^T R_k + \alpha(D_x^T S_x D_x + D_y^T S_y D_y) + \lambda \mathbf{1}}, \tag{15}$$

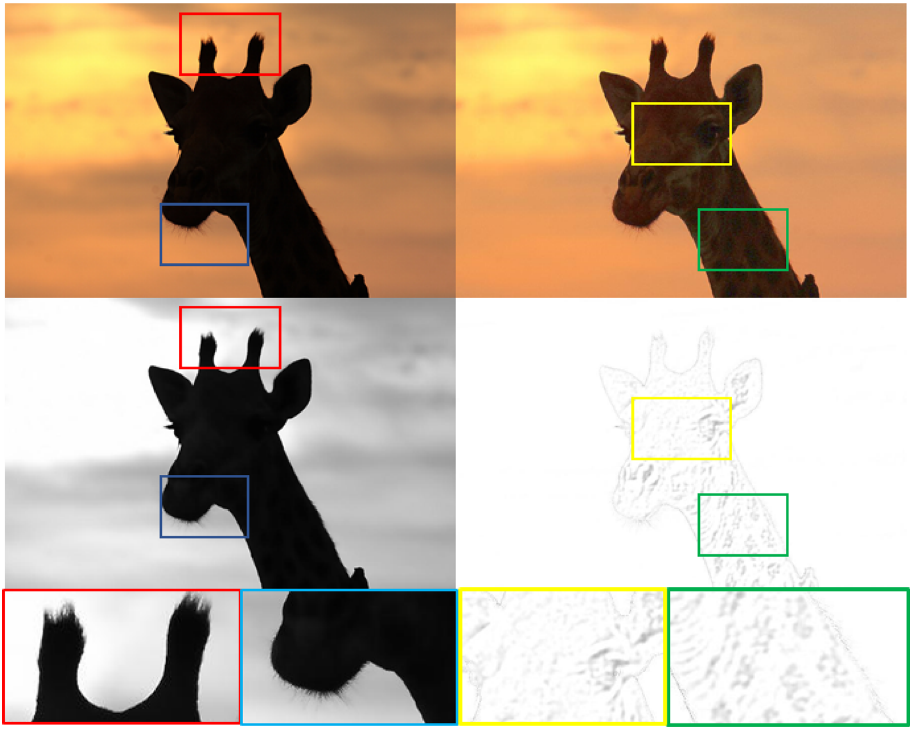

**Fig. 3** Structure and texture extracted by the STR$^2$ model. The first row represents the input image and the enhanced result, the second row depicts the structure map and texture map, and the third row shows the details

where **1** is an identity matrix.

**2**) ***R* Sub-problem** We initialize the $R_0 = I/L_1$ and update $R$ while fixing $L$. The terms unrelated to $R$ are neglected, and the solution to update $(k+1)$-th iteration $R_{k+1}$ is derived as

$$R_{k+1} = \arg\min_{R_k} \|I - L_{k+1} \odot R_k\|_F^2 + \beta(t_x \|\nabla_x R_k\|_F^2 + t_y \left\|\nabla_y R_k\right\|_F^2). \tag{16}$$

Then, the loss function to the matrix notation is reformulated as

$$\begin{aligned} R_{k+1} &= (L_{k+1} \odot R_k - I)^T (L_{k+1} \odot R_k - I) \\ &+\beta(R_k^T D_x^T T_x D_x R_k + R_k^T D_y^T T_y D_y R_k), \end{aligned} \tag{17}$$

where $T_x = diag(t_x)$ and $T_y = diag(t_y)$.

The solution to (16) is

$$R_{k+1} = \frac{L_{k+1}^T I}{L_{k+1}^T L_{k+1} + \beta(D_x^T T_x D_x + D_y^T T_y D_y)}. \tag{18}$$

The cycled optimization continues until the convergence conditions [61] are satisfied or the rounds of iteration reach a pre-defined threshold. A summary of the optimization method for the proposed STR$^2$ model is demonstrated in Algorithm 1.

**Input**: Observed image $I$, parameters $\gamma_s$, $\gamma_t$, $\alpha$, $\beta$ and $\lambda$, maximum iterations $K$ and stopping parameters $\delta$.
Initializing $L_0$ and $R_0$, and setting the structure and texture weight matrices $\mathcal{S}_0$ and $\mathcal{T}_0$
**for** $k = 1 : K$ **do**
    **1.** Compute structure weight $\mathcal{S}_{k+1}$ by Eq. (11)
    **2.** Update $L_{k+1}$ by Eq. (15)
    **3.** Compute texture weight $\mathcal{T}_{k+1}$ by Eq. (12)
    **4.** Update $R_{k+1}$ by Eq. (18)
    **if** $\|L_{k+1} - L_k\|_F \,/\, \|L_k\|_F \leq \delta$ *or* $\|R_{k+1} - R_k\|_F \,/\, \|R_k\|_F \leq \delta$ **then**
        Stop Updating
        **else**
            Continue
        **end**
    **end**
**end**
Estimate $\hat{O}$ by Eq. (20)
**Output**: Enhanced RGB image $\hat{O}$

**Algorithm 1** The optimization of the proposed STR$^2$ model.

To verify the convergence of the Algorithm 1, the convergence analysis is carried out on the VV dataset[1]. The errors of $\|L_{k+1} - L_k\|_F \,/\, \|L_k\|_F$ and $\|R_{k+1} - R_k\|_F \,/\, \|R_k\|_F$ are calculated, and their curves are drawn in Fig. 4. It shows that both of them drop below 0.005 after 20 iterations. Thus, three optional convergence conditions for Algorithm 1 are derived as follows.

- $\|L_{k+1} - L_k\|_F \,/\, \|L_k\|_F \leq 0.005$
- $\|R_{k+1} - R_k\|_F \,/\, \|R_k\|_F \leq 0.005$
- The iteration number $K = 20$

### 4.4 Illumination adjustment

Since the brightness information is contained by the illumination component of the image, it is possible to adjust the illumination component to generate a visually satisfying result for a low-light image. After obtaining the enhanced components of the illumination $L$ and the reflectance $R$, the goal is to adjust $L$ to improve the visibility and brightness of the input image. Therefore, in this paper, we adopt the Gamma correction [44, 58] to adjust the illumination component. The corrected illumination is written as

$$\hat{L} = L^{\frac{1}{\gamma}}. \tag{19}$$

[1] https://sites.google.com/site/vonikakis/datasets

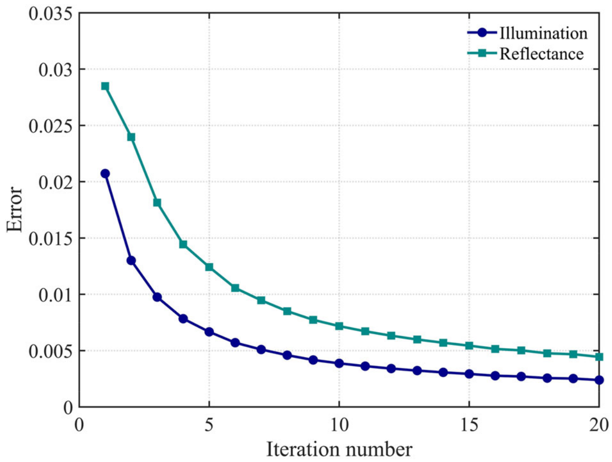


**Fig. 4** Convergence analysis on VV dataset. The curves are obtained by averaging $\|L_{k+1} - L_k\|_F \,/\, \|L_k\|_F$ and $\|R_{k+1} - R_k\|_F \,/\, \|R_k\|_F$ in the iterative process

The enhanced result $\hat{O}$ is generated by

$$\hat{O} = R \odot L^{\frac{1}{\gamma}}, \tag{20}$$

where $\gamma = 2.2$ is an empirical value [13, 16]. Finally, the enhanced image is generated by reversing from HSV to RGB.

## 5 Experimental results and analysis

In this section, the experiment settings and implementation details are given first. Then the comparison results with the state-of-the-art (SOTA) methods are presented in both subjective and objective aspects. Subsequently, we perform ablation studies to assess the impact of the key parameters. Finally, we discussed the computational complexity of the proposed method.

### 5.1 Experiment settings and implementation details

The experiments are performed on a PC with an Intel i5-10400 CPU, 2.90GHz and 16GB memory. We set the parameters as $\gamma_s = 1.0$, $\gamma_t = 0.75$, $\alpha = 0.001$, $\beta = 0.0001$, $\delta = 0.005$, and $\lambda = 0.25$. For a fair comparison, the results of the competitors are reproduced by official codes.

Comparative experiments are performed on 7 benchmark datasets, *i.e.*, LIME [20], DICM [30], MEF [41], NPE [56], LOL [57], LOE [63] and VV[2]. Meanwhile, we carry out experiments on 35 challenging images with different lighting conditions collected from previous works [10–12, 20, 50, 56]. The proposed STR[2] are compared with 14 competitors, including HE [15], Dong [9], CVC [70], LDR [31], SSR [23], MSRCR [48],

[2] https://sites.google.com/site/vonikakis/datasets

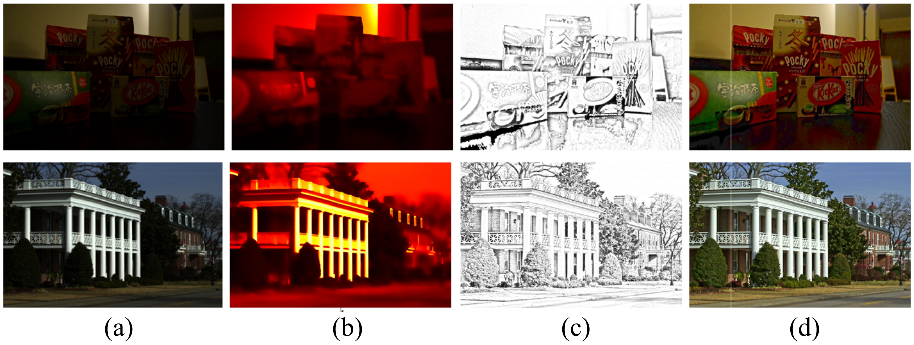

**Fig. 5** The Retinex decomposition results by the STR$^2$. (a) low light images, (b) illumination maps, (c) reflectance maps, (d) enhanced results

NPE [56], MF [11], LIME [20], Jiep [4], STAR [61], SGZ [69], RetinexDIP [68], and ZERO-DCE++ [33].

### 5.2 Retinex decomposition analysis

The results of the Retinex decomposition of STR$^2$ are shown in Fig. 5. As mentioned in Section 1, the illumination map should be piece-wise smooth while maintaining the structure of objects. Considering the illumination map in the first row, it contains the edge of the packing boxes and maps the illumination distribution across the wall and desk. The reflectance map in the second row extracts the texture of trees properly. Overall, the STR$^2$ could generate appropriate Retinex decomposition results.

**Fig. 6** Images for the qualitative evaluation under different low-light conditions

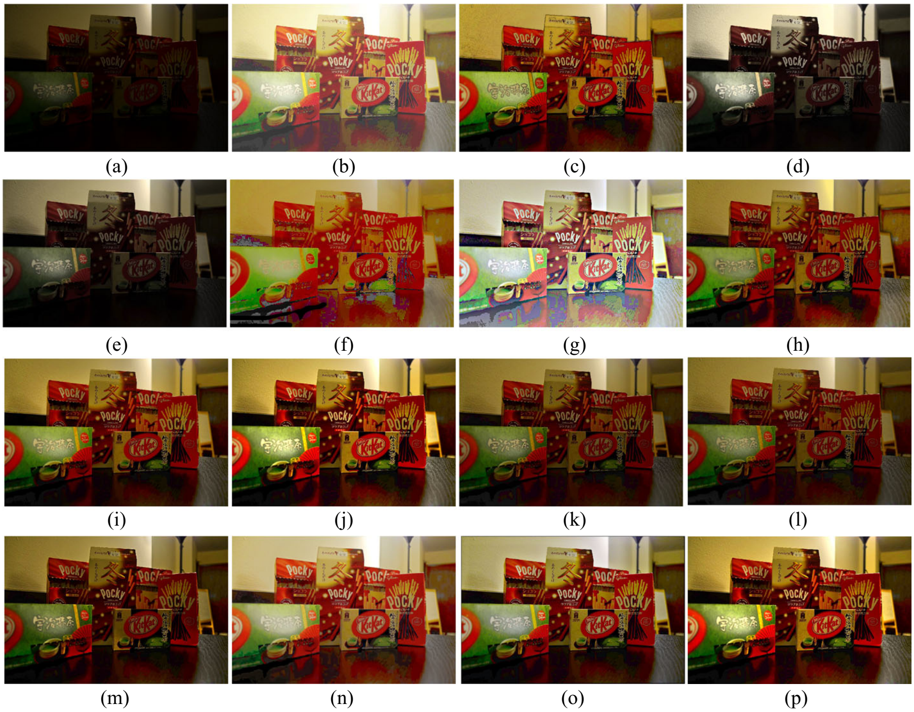


**Fig. 7** Visual evaluation of an image with the SOTA methods. (a) Input (b) HE [15], (c) Dong [9], (d) CVC [70], (e) LDR [31], (f) SSR [23], (g) MSRCR [48], (h) NPE [56], (i) MF [11], (j) LIME [20], (k) Jiep [4], (l) STAR [61], (m) RetinexDIP [68], (n) SGZ [69], (o)ZERO-DCE++ [33], (p) Ours

### 5.3 Qualitative evaluation

In this subsection, we provide a subjective evaluation of the proposed method. Numerous images under different low-light conditions are tested, among which six representative images with backlighting, low-light and non-uniform illumination are shown in Fig. 6. The enhanced results are depicted from Figs. 7, 8, 9, 10, 11 and 12.

As stated by Chen et al. [5], image enhancement methods should avoid dramatic alternation of lighting conditions to the scene, and should not introduce additional artifacts or amplify hidden distortions of images. The ambiance of the image (warm or cold color impression) should not be changed greatly after enhancement. Following the criteria, we take the compare between visual evaluation examples. Based on the criteria above, the subjective results are analyzed as follows.

The results based on HE [15] tend to be under the same illumination level globally, which causes the enhancement of the image. In Fig. 12 (b), the image is overly enhanced, and the hidden noise is amplified. Dong [9] is effective in improving the brightness, but the details of the enhanced images are under excessive enhancement. For example, the text on the packing box in Fig. 7 (c) and the outline of the flowers in Fig. 9 (c) are overly bold. The HE-based methods LDR [31] and CVC [70] perform well in preserving the details, but cannot improve the brightness effectively. For example, in Fig. 7 (d), the brightness is barely enhanced compared with the original image. The results based on the SSR [23] suffer from distortions, *e.g.*, unrealistic edges, strongly boosted noise, and color distortion. In Fig. 12

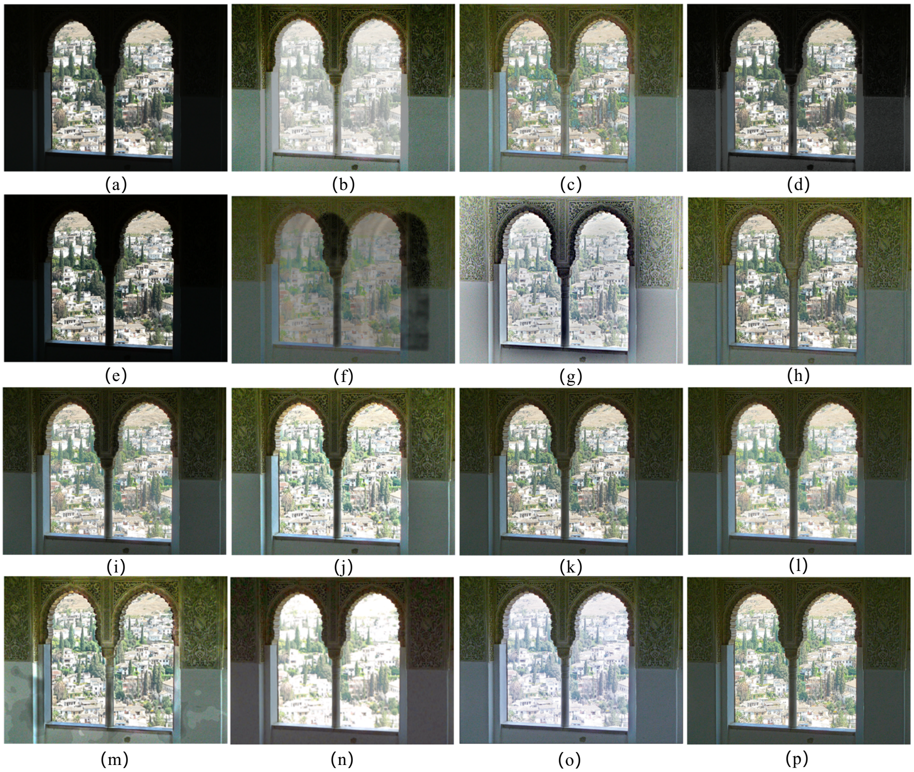

**Fig. 8** Visual evaluation of an image with the SOTA methods. (a) Input (b) HE [15], (c) Dong [9], (d) CVC [70], (e) LDR [31], (f) SSR [23], (g) MSRCR [48], (h) NPE [56], (i) MF [11], (j) LIME [20], (k) Jiep [4], (l) STAR [61], (m) RetinexDIP [68], (n) SGZ [69], (o)ZERO-DCE++ [33], (p) Ours

(f), the lighting condition is dramatically alternated, and the color is distorted. MSRCR [48] can improve the brightness of the image while maintaining clear details, but it changes the ambiance of the image greatly. For instance, in Fig. 11 (g), the details such as the distant buildings outside the window and patterns on the walls have been well-preserved, but the color of the whole picture is severely distorted. LIME [20] may cause over-enhancement and noise amplification in enhanced results. For instance, the building captured through the window is blurred in Fig. 8 (j) and the noise in the dark background is amplified in Fig. 8 (j). ZERO-DCE++ [33] could generate bright and detail-maintained enhanced results, but the ambiance of the image is destroyed. For example, in Fig. 9 (m) and (n), the color of the flower is distorted. RetinexDIP [68] could achieve the effective lightness enhancement of dark background, *e.g.*, in Fig. 12 (m) the people and the table in the background are brightened. But in Fig. 8, the dark front region tends to be blurry. SGZ may generate unsatisfactory results on images with large differences in brightness distribution, *e.g.*, Figs. 8 (n) and 12 (n). Comparatively speaking, the methods of NPE [56], MF [11], JieP [4], STAR [61] and the proposed STR$^2$ can achieve acceptable visual quality in the images.

Different enhancement methods may produce different subjective results. The quality of the results depends largely on the individual's subjective judgment. Thus, it is difficult to

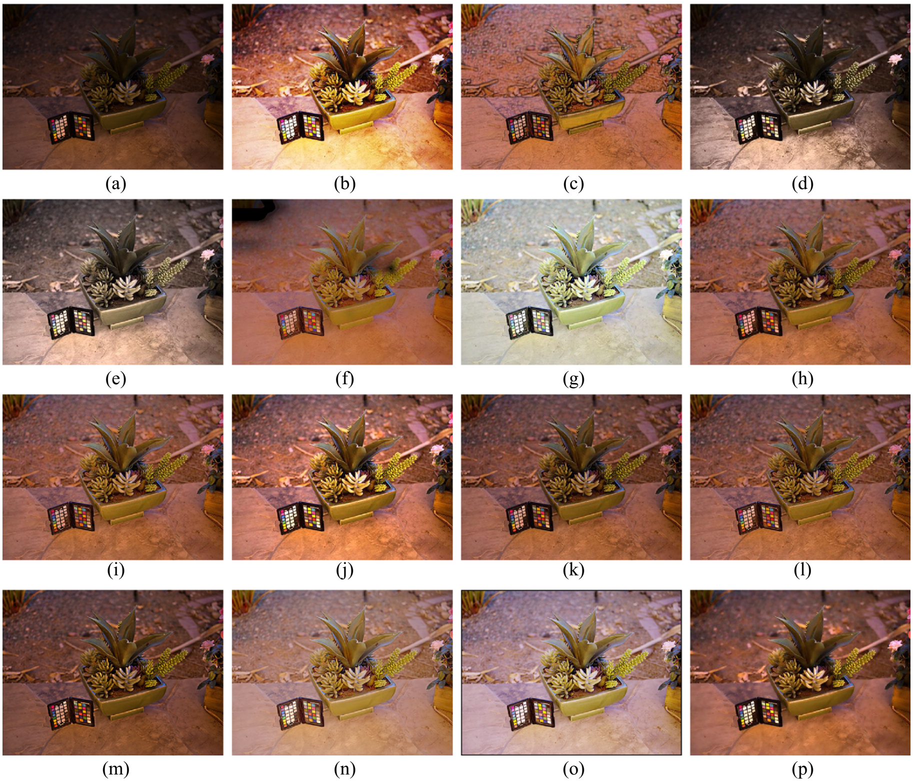


**Fig. 9** Visual evaluation of an image with the SOTA methods. (a) Input (b) HE [15], (c) Dong [9], (d) CVC [70], (e) LDR [31], (f) SSR [23], (g) MSRCR [48], (h) NPE [56], (i) MF [11], (j) LIME [20], (k) Jiep [4], (l) STAR [61], (m) RetinexDIP [68], (n) SGZ [69], (o)ZERO-DCE++ [33], (p) Ours

compare the enhancement effect on the enhanced images, especially for the subtle difference. Therefore, we conduct quantitative analysis and comparison of the enhanced images generated by the SOTA methods in Section 5.4.

### 5.4 Quantitative evaluation

Since the evaluation of enhanced images is highly correlative to human visual perception, it's a dilemma to employ a general method to evaluate the quality of an image. Generally speaking, the methods of image quality assessment (IQA) can be divided into two categories, *i.e.,* full reference-based methods and no reference-based methods [17, 19]. Considering that there is a rare ground truth image in the dataset, we employ two non-reference-based IQAs (*i.e.*, Natural Image Quality Evaluator (NIQE) [42] and the sharpness metric in the autoregressive parameter space (a.k.a. "ARISMC") [18]).

The NIQE indicator evaluates the difference in feature distribution between a natural image dataset and a testing dataset [42]. A lower NIQE value means that the gap between the enhanced image and the natural image is smaller and the quality of the image is better.

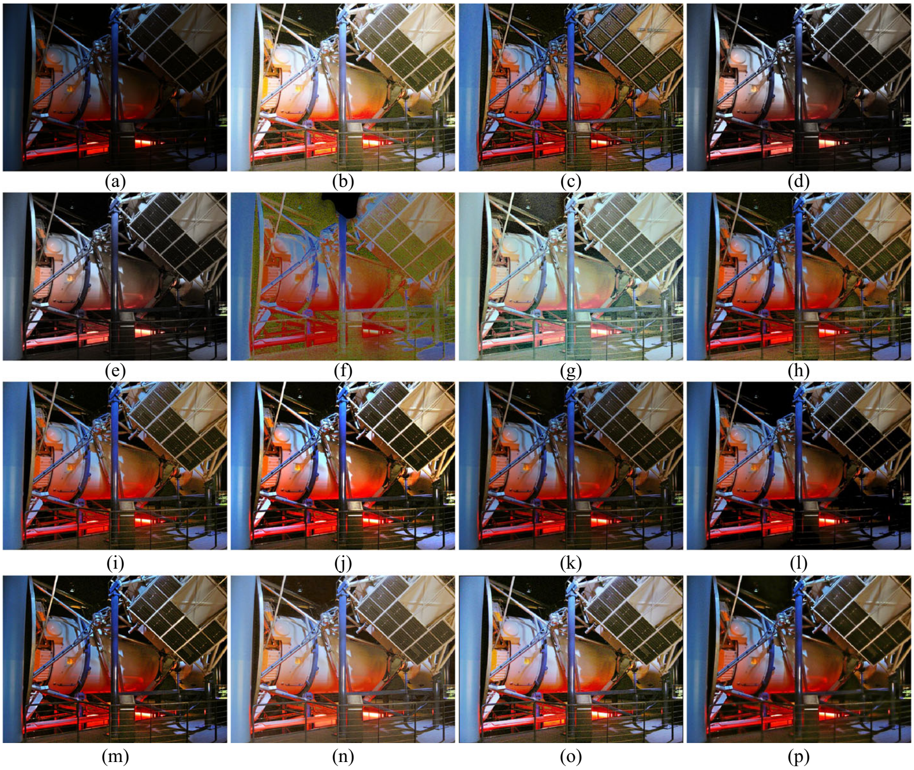


**Fig. 10** Visual evaluation of an image with the SOTA methods. (a) Input (b) HE [15], (c) Dong [9], (d) CVC [70], (e) LDR [31], (f) SSR [23], (g) MSRCR [48], (h) NPE [56], (i) MF [11], (j) LIME [20], (k) Jiep [4], (l) STAR [61], (m) RetinexDIP [68], (n) SGZ [69], (o)ZERO-DCE++ [33], (p) Ours

The formula of NIQE is given as:

$$\mathrm{NIQE}\left(v_1, v_2, \xi_1, \xi_2\right) = \sqrt{\left(v_1 - v_2\right)^{\mathrm{T}} \left(\frac{\xi_1 + \xi_2}{2}\right)^{-1} \left(v_1 - v_2\right)}, \tag{21}$$

where $v_1$, $v_2$, $\xi_1$, $\xi_2$ represent the mean of the specific natural image dataset and the test image and their corresponding variances. However, the NIQE indicator solely focuses on whether the texture information is consistent with the characteristics of the natural image, and the color ambiance information (*e.g.*, warm and cold) is often ignored. To address this issue, we choose ARISMC as an auxiliary indicator. Based on the parameter analysis of the classical auto regressive (AR) image model, ARISMC is to estimate the image sharpness considering both luminance and chromatic components [18]. The formula of ARISMC is given as:

$$ARISMC = \sum_{k \in \Psi} \Theta_k \cdot \rho_k, \tag{22}$$

where $\Psi = \left\{E, C, E^{bb}, C^{bb}\right\}$. $E, C, E^{bb}, andC^{bb}$ are the local sharpness estimation, local contrast estimation, block-based sharpness estimation and block-based contrast estimation, respectively. The sharpness score is computed by averaging the largest $\mathcal{Q}_k\%$ values in the $k$

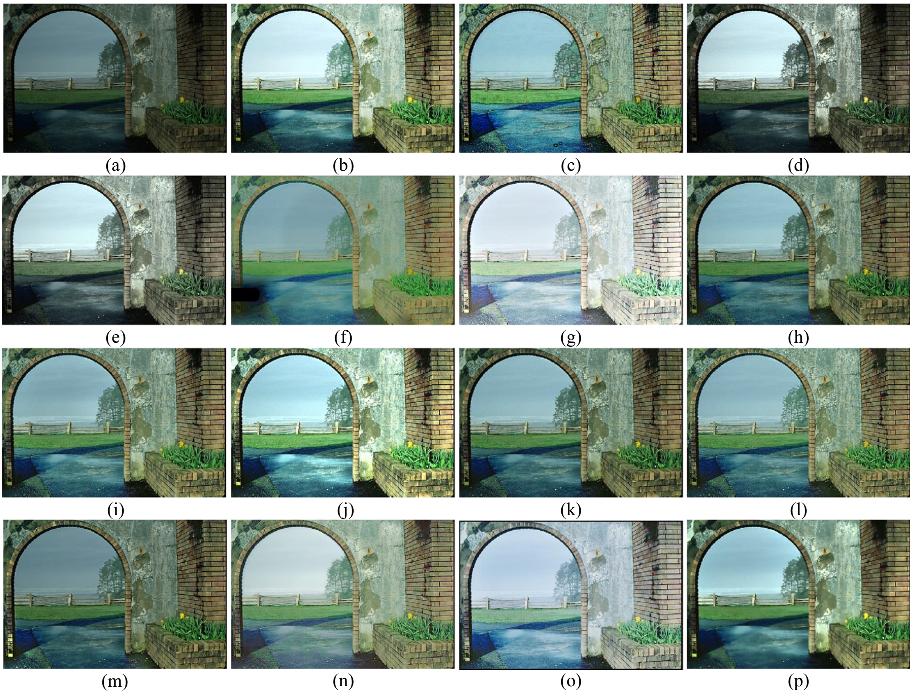

**Fig. 11** Visual evaluation of an image with the SOTA methods. (a) Input (b) HE [15], (c) Dong [9], (d) CVC [70], (e) LDR [31], (f) SSR [23], (g) MSRCR [48], (h) NPE [56], (i) MF [11], (j) LIME [20], (k) Jiep [4], (l) STAR [61], (m) RetinexDIP [68], (n) SGZ [69], (o)ZERO-DCE++ [33], (p) Ours

$\left(k \in \left\{E, C, E^{bb}, C^{bb}\right\}\right)$ map. $\mathcal{Q}_k\%$ is overall sharpness average parameter. $\Theta_k$ is the positive constant used to adjust the relative importance of each component. A smaller ARISMC value means an image with higher sharpness, less blur, and higher quality.

Quantitative comparisons in terms of NIQE and ARISMC are shown in Tables 1 and 2, respectively. The best, second-best and third-best results are highlighted in red, blue and green, respectively. As reported in Table 1, the STR$^2$ ranks first place on the LIME dataset, the second-best place on 35 image datasets, and the third-best place on LOL datasets, respectively. Although the proposed method does not achieve the top-3 results on the other four datasets, it can be comparable to the deep learning-based methods, *i.e.*, RetinexDIP, SGZ and ZERO-DCE++. Overall, the STR$^2$ achieves the third-best in average score, which outperforms the deep learning-based methods and the STAR. Table 2 reports the results among the competitors in terms of ARISMC. It shows that the STR$^2$ ranks second-best place on LIME and LOE datasets, and third-best place on LOL, MEF and VV datasets, respectively. The proposed method achieves an average score of 1.1893 which ranks the third-best place. It outperforms the deep learning-based methods, and it is very close to the STAR (1.1818).

### 5.5 Impact of key parameters

We compare the influence of different groups of parameter choices on Retinex decomposition and enhancement results to evaluate the impact of key parameters. In ablation studies,

**Table 1** Quantitative comparisons in terms of NIQE

| Methods \ Datasets | LIME [20] | 35 images | DICM [30] | NPE [56] | LOE [63] | LOL [57] | MEF [41] | VV | Average |
|---|---|---|---|---|---|---|---|---|---|
| HE [15] | 4.1654 | 3.4502 | 3.5547 | 3.3017 | 4.9219 | 4.9530 | 2.6841 | 2.6189 | 3.7062 |
| Dong [9] | 4.3240 | 4.0932 | 3.7747 | 4.2652 | 4.4903 | 3.8842 | 3.4191 | 3.0550 | 3.9132 |
| CVC [70] | 3.7775 | 3.1431 | 2.8245 | 3.1351 | 4.7309 | 5.1495 | 2.8315 | 2.3585 | 3.4938 |
| LDR [31] | 4.0028 | 3.1585 | 2.8502 | 3.1610 | 5.0595 | 4.0060 | 2.9670 | 2.5497 | 3.4693 |
| SSR [23] | 4.2358 | 3.2540 | 3.4375 | 3.1238 | 4.4214 | 4.1085 | 2.7745 | 2.7951 | 3.5188 |
| MSRCR [48] | 3.9516 | 3.2386 | 3.3319 | 3.3562 | 3.9347 | 4.2907 | 2.7104 | 2.5460 | 3.4200 |
| NPE [56] | 4.0751 | 3.2635 | 3.2256 | 3.2540 | 4.3179 | 4.3507 | 2.7394 | 2.5865 | 3.4766 |
| MF [11] | 4.1301 | 3.3805 | 3.1081 | 3.3805 | 4.8837 | 4.2423 | 2.7499 | 2.4428 | 3.5397 |
| LIME [20] | 4.5209 | 3.4790 | 3.2488 | 3.4821 | 4.7246 | 4.1112 | 2.8096 | 2.4500 | 3.6033 |
| JieP [4] | 3.9273 | 3.2071 | 2.7631 | 3.2980 | 4.7132 | 3.1198 | 2.7999 | 2.5132 | 3.2927 |
| STAR [61] | 3.8889 | 3.5868 | 4.2457 | 3.9057 | 4.7266 | 2.9392 | 2.8067 | 2.5912 | 3.5864 |
| RetinexDIP [68] | 3.1679 | 3.3743 | 3.8595 | 3.4714 | 4.3691 | 6.9582 | 3.3520 | 2.1211 | 3.8342 |
| SGZ [69] | 3.7769 | 3.4491 | 3.1599 | 3.1105 | 3.5747 | 6.1343 | 2.8946 | 2.4508 | 3.5688 |
| ZERO-DCE++ [33] | 3.8074 | 3.6858 | 3.1414 | 3.1329 | 3.5488 | 6.1962 | 2.8818 | 2.4481 | 3.6053 |
| Ours | 3.6212 | 3.1552 | 3.0632 | 3.3322 | 4.6490 | 3.3730 | 3.6340 | 2.7914 | 3.4524 |

The best, the second-best and the third-best results are highlighted in red, blue and green, respectively

**Table 2** Quantitative comparisons in terms of ARISMC

| Methods \ Datasets | LIME [20] | 35 images | DICM [30] | NPE [56] | LOE [63] | LOL [57] | MEF [41] | VV | Average |
|---|---|---|---|---|---|---|---|---|---|
| HE [15] | 1.2903 | 1.2843 | 1.2997 | 1.2762 | 1.1776 | 1.2986 | 1.2637 | 1.2313 | 1.2652 |
| Dong [9] | 1.2700 | 1.3040 | 1.2771 | 1.3142 | 1.1836 | 1.2712 | 1.2716 | 1.2696 | 1.2702 |
| CVC [70] | 1.2445 | 1.2543 | 1.2410 | 1.2563 | 1.1453 | 1.2877 | 1.2218 | 1.2044 | 1.2319 |
| LDR [31] | 1.2255 | 1.2223 | 1.2059 | 1.2395 | 1.0670 | 1.2700 | 1.1966 | 1.1720 | 1.1998 |
| SSR [23] | 1.2378 | 1.2297 | 1.2289 | 1.2385 | 1.1176 | 1.2726 | 1.1957 | 1.1695 | 1.2113 |
| MSRCR [48] | 1.3019 | 1.2981 | 1.3164 | 1.2954 | 1.2074 | 1.3112 | 1.2876 | 1.2776 | 1.2870 |
| NPE [56] | 1.2263 | 1.2469 | 1.2421 | 1.2577 | 1.1634 | 1.2984 | 1.2206 | 1.2154 | 1.2339 |
| MF [11] | 1.2476 | 1.2822 | 1.2739 | 1.2915 | 1.1343 | 1.2973 | 1.2439 | 1.2463 | 1.2521 |
| LIME [20] | 1.2782 | 1.2880 | 1.2753 | 1.2975 | 1.1729 | 1.2860 | 1.2594 | 1.2388 | 1.2620 |
| JieP [4] | 1.2009 | 1.2405 | 1.2218 | 1.2637 | 1.0544 | 0.9035 | 1.2177 | 1.2152 | 1.1647 |
| STAR [61] | 1.2288 | 1.2527 | 1.2193 | 1.2559 | 1.0741 | 0.9898 | 1.2240 | 1.2094 | 1.1818 |
| RetinexDIP [68] | 1.2667 | 1.2720 | 1.2494 | 1.2905 | 1.1269 | 1.1011 | 1.2560 | 1.2298 | 1.2240 |
| SGZ [69] | 1.2600 | 1.2689 | 1.2523 | 1.2806 | 1.1084 | 1.2230 | 1.2359 | 1.1951 | 1.2280 |
| ZERO-DCE++ [33] | 1.2654 | 1.2720 | 1.2536 | 1.2772 | 1.1263 | 1.2420 | 1.2415 | 1.2028 | 1.2351 |
| Ours | 1.2250 | 1.2432 | 1.2302 | 1.2615 | 1.0631 | 1.0944 | 1.2126 | 1.1842 | 1.1893 |

The best, the second-best and the third-best results are highlighted in red, blue and green, respectively

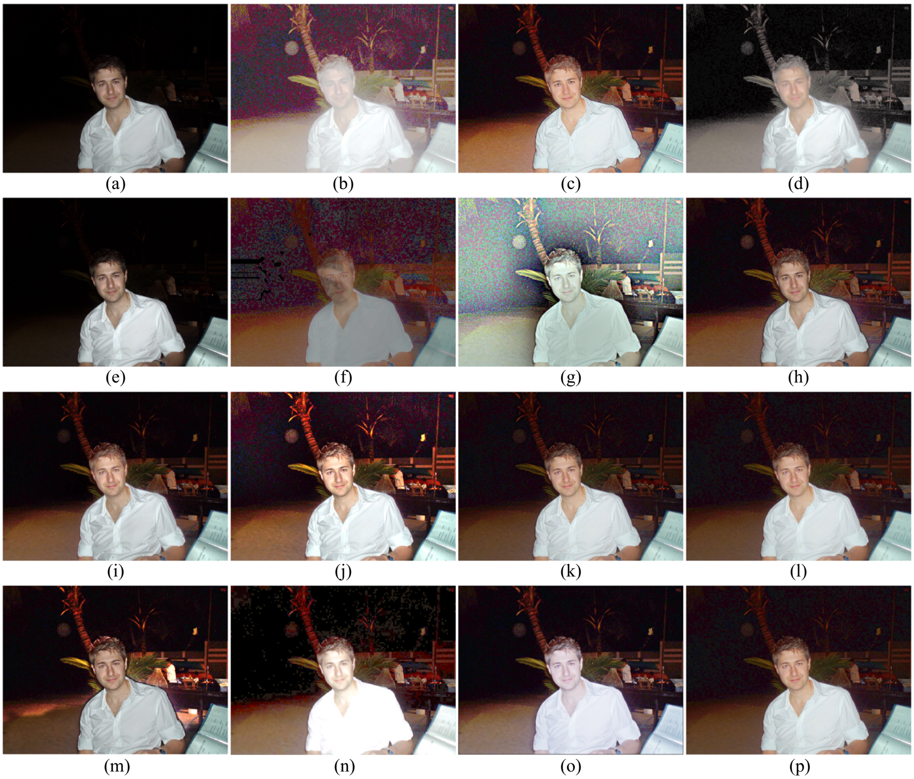

**Fig. 12** Visual evaluation of an image with the SOTA methods. (a) Input (b) HE [15], (c) Dong [9], (d) CVC [70], (e) LDR [31], (f) SSR [23], (g) MSRCR [48], (h) NPE [56], (i) MF [11], (j) LIME [20], (k) Jiep [4], (l) STAR [61], (m) RetinexDIP [68], (n) SGZ [69], (o)ZERO-DCE++ [33], (p) Ours

the illumination map is expected to be smooth while the structure is maintained. For the reflectance component, the texture information should be extracted.

1) $\gamma_s$ and $\gamma_t$. Since the coefficients of $\gamma_s$ and $\gamma_t$ in (6) and (7) play a decisive role on structure and texture awareness in the proposed model, it's pivotal to determine the reasonable values of them. Figure 13 demonstrates the subjective comparisons of the illumination and reflectance with different pairs of $(\gamma_s, \gamma_t)$. It shows that the illumination map is getting smoother along with the increase of $\gamma_s$. On the contrary, with the increase of $\gamma_t$, the proposed STR$^2$ performs better on the extraction of texture information. In order to achieve mutually satisfactory effects, these two parameters should be balanced against each other. In Fig. 13, the model with $\gamma_s = 1.25$ and $\gamma_s = 1.5$ can barely distinguish the structure from illumination or extract the texture from reflectance. In Fig. 13 (a) and (b), the model with $\gamma_s = 0.75$ fails to enhance the spatial smooth of illumination. Overall, the model with $\gamma_s = 1.0$ and $\gamma_t = 0.75$ (Fig. 13 (c)) will achieve satisfied results.

2) $\alpha$ and $\beta$. The coefficients of $\alpha$ and $\beta$ are the weight parameter of illumination and reflectance components. To determine reasonable values of these two parameters, Retinex decomposition experiments are performed on the 'building' image.

The illumination and reflectance components of the STR$^2$ Retinex decomposition with different values of $\alpha$ and $\beta$ ($\alpha, \beta \in \{0.1, 0.01, 0.001, 0.0001\}$) are shown in Fig. 14. It shows

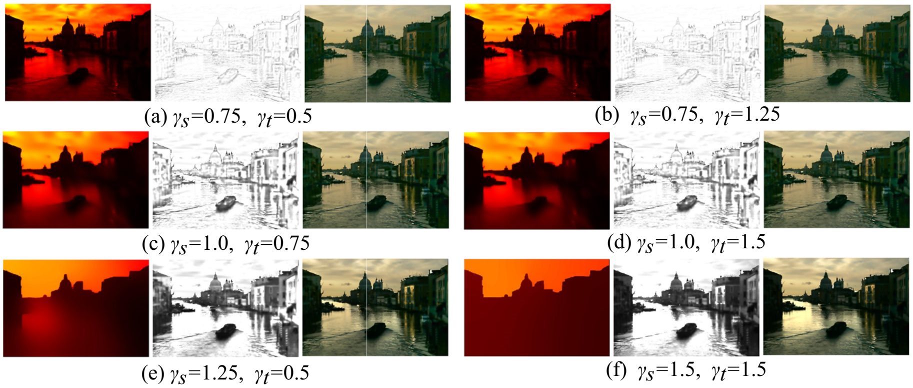


**Fig. 13** Comparison of decomposition component and enhanced result with different $(\gamma_s, \gamma_t)$ on the image "Venice" from MEF dataset

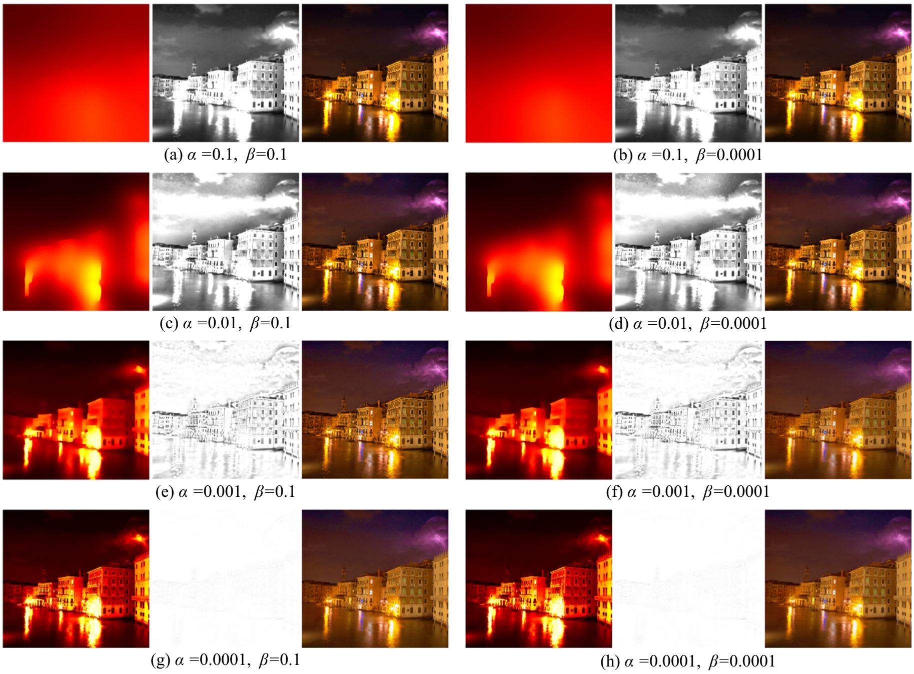


**Fig. 14** Comparison of decomposition component and enhanced result with different $\alpha$ and $\beta$ on the 'building' image from the LIME dataset

that the decomposition results are more sensitive to the variation of $\alpha$ than $\beta$. In Fig. 14 (a) and (b), the illumination maps tend to be obscure, and the reflectance maps fail to extract the texture information. In Fig. 14(g), there is little difference between the illumination component and the $V$ channel. We observe that the model with $\alpha = 0.001$ and $\beta = 0.0001$ produces optimal results.

**Fig. 15** Failure cases of the proposed STR$^2$ model. The first row is the low-light image, and the second row is the enhanced result

### 5.6 Computational complexity

The computational time is calculated by averaging the process time of ten images which are resized to $960 \times 720$ and the results of comparison are depicted in Table 3. It shows that the proposed method requires more running time than the majority of the methods, but the enhanced results of the proposed method achieve satisfied qualitative and quantitative effects. It is worth mentioning that the processing is simply iterated without optimization in this paper, and it can be accelerated by adopting optimization algorithms such as alternating direction minimizing (ADM) [55, 60]. Furthermore, the processing speed of the MATLAB code can be accelerated by adopting C/C++ programming and employing GPUs.

### 5.7 Failure case study

In some cases, the performances of the proposed STR$^2$ are not very satisfactory. Some failure examples are shown in Fig. 15. In these examples, the low-light images have dark backgrounds and numerous light sources. At the same time, these abounded light sources often introduce halo effects in low-light images. The structure prior can't handle such severe distortion of the illumination map. Besides the aforementioned reasons, numerous bright and dark boundary between the light source and the dark background makes the structure prior fail to deal with the gradient of the illumination component. In the follow-up work, more efforts are expected to solve this problem.

**Table 3** Comparison of time cost (in second)

| Method | Dong [9] | CVC [70] | SSR [23] | MSRCR [48] | NPE [56] |
|---|---|---|---|---|---|
| Time | 2.62 | 0.79 | 2.17 | 6.67 | 28.71 |
| Method | MF [11] | LIME [20] | Jiep [4] | STAR [61] | Ours |
| Time | 2.31 | 14.11 | 13.43 | 21.80 | 18.90 |

## 6 Conclusion

In this paper, we build a Structure and Texture Revealing Retinex ($STR^2$) model for low-light image enhancement. We explore the structure and texture constraints to enforce the spatial smooth on the illumination layer and piece-wise continuous on reflectance layer, respectively. The key idea is to accurately estimate the structure and texture maps via analysing the difference of gradient distribution in illumination and reflectance layers. To this aim, an alternative update algorithm is developed to solve the model. The effectiveness of the proposed model is verified on public benchmarks, and comparative results show that our method performs favorably against many state-of-the-art methods in terms of low-light image enhancement.

**Acknowledgements** This work is supported in part by the National Natural Science Foundation of Shandong Province (Nos. ZR2021QD041 and ZR2020MF127).

### Declarations

**Conflict of Interests** The authors declare that they have no conflict of interest

## References

1. Arici T, Dikbas S, Altunbasak Y (2009) A histogram modification framework and its application for image contrast enhancement. IEEE Trans Image Process 18:1921–1935
2. Brainard D, Wandell B (1986) Analysis of the retinex theory of color vision. J Optical Soc Am A, Optics Image Sci 3(10):1651–61
3. Bychkovsky V, Paris S, Chan E, Durand F (2011) Learning photographic global tonal adjustment with a database of input/output image pairs. In: CVPR 2011, pp 97–104
4. Cai B, Xu X, Guo K, Jia K, Hu B, Tao D (2017) A joint intrinsic-extrinsic prior model for retinex. In: Proceedings of the international conference on computer vision (ICCV), pp 4020–4029
5. Chen S, Beghdadi A (2009) Natural rendering of color image based on retinex. In: 2009 16th IEEE international conference on image processing (ICIP), pp 1813–1816. IEEE
6. Chen C, Chen Q, Xu J, Koltun V (2018) Learning to see in the dark. In: 2018 IEEE/CVF Conference on computer vision and pattern recognition, pp 3291–3300
7. Chen L, Yang X, Jeon G, Anisetti M, Liu K (2020) A trusted medical image super-resolution method based on feedback adaptive weighted dense network. Artif Intell Med 106:101857
8. Chen J, Yang X, Lu L, Li Q, Li Z, Wu W (2020) A novel infrared image enhancement based on correlation measurement of visible image for urban traffic surveillance systems. J Intell Transp Syst 24(3):290–303
9. Dong X, Pang Y, Wen J (2011) Fast efficient algorithm for enhancement of low lighting video. In: 2011 IEEE International conference on multimedia and expo, pp 1–6
10. Fu X, Liao Y, Zeng D, Huang Y, Zhang X, Ding X (2015) A probabilistic method for image enhancement with simultaneous illumination and reflectance estimation. IEEE Trans Image Process 24:4965–4977
11. Fu X, Zeng D, Huang Y, Liao Y, Ding X, Paisley J (2016) A fusion-based enhancing method for weakly illuminated images. Signal Process 129:82–96
12. Fu X, Zeng D, Huang Y, Zhang X, Ding X (2016) A weighted variational model for simultaneous reflectance and illumination estimation. In: Proceedings of the IEEE computer vision and pattern recognition (CVPR), pp 2782–2790
13. Gao Y, Hu HM, Li B, Guo Q (2018) Naturalness preserved nonuniform illumination estimation for image enhancement based on retinex. IEEE Trans Multimed 20:335–344
14. Gharbi M, Chen J, Barron JT, Hasinoff S, Durand F (2017) Deep bilateral learning for real-time image enhancement. ACM Transactions on Graphics (TOG) 36:1–12
15. González R, Woods R (1981) Digital image processing. IEEE Trans Pattern Anal Mach Intell PAMI-3, pp 242–243
16. Gu Z, Li F, Fang F, Zhang G (2020) A novel retinex-based fractional-order variational model for images with severely low light. IEEE Trans Image Process 29:3239–3253

17. Gu K, Lin W, Zhai G, Yang X, Zhang W, Chen C (2017) No-reference quality metric of contrast-distorted images based on information maximization. IEEE Trans Cybern 47:4559–4565
18. Gu K, Zhai G, Lin W, Yang X, Zhang W (2015) No-reference image sharpness assessment in autoregressive parameter space. IEEE Trans Image Process 24:3218–3231
19. Gu K, Zhai G, Yang X, Zhang W (2015) Using free energy principle for blind image quality assessment. IEEE Trans Multimed 17:50–63
20. Guo X, Li Y, Ling H (2017) Lime: Low-light image enhancement via illumination map estimation. IEEE Trans Image Process 26:982–993
21. Ibrahim H, Kong N (2007) Brightness preserving dynamic histogram equalization for image contrast enhancement. IEEE Trans Consum Electron, p 53
22. Jiang Y, Gong X, Liu D, Cheng Y, Fang C, Shen X, Yang J, Zhou P, Wang Z (2021) Enlightengan: Deep light enhancement without paired supervision. IEEE Trans Image Process 30:2340–2349
23. Jobson D, Rahman Z, Woodell G (1997) Properties and performance of a center/surround retinex. IEEE Trans Image Process 6(3):451–462. 10.1109/83.557356
24. Jobson DJ, Rahman Z, Woodell GA (1997) A multiscale retinex for bridging the gap between color images and the human observation of scenes. IEEE Trans Image Process:, A Publication of the IEEE Signal Processing Society 6(7):965–76
25. Khan MF, Khan E, Abbasi Z (2015) Image contrast enhancement using normalized histogram equalization. Optik 126(24):4868–4875
26. Kim G, Kwon D, Kwon J (2019) Low-lightgan: Low-light enhancement via advanced generative adversarial network with task-driven training. In: 2019 IEEE International conference on image processing (ICIP), pp 2811–2815. IEEE
27. Kim G, Park SW, Kwon J (2021) Pixel-wise wasserstein autoencoder for highly generative dehazing. IEEE Trans Image Process 30:5452–5462
28. Kimmel R, Elad M, Shaked D, Keshet R, Sobel I (2004) A variational framework for retinex. Int J Comput Vis 52:7–23
29. Land E (1977) The retinex theory of color vision. Sci Am 237(6):108–28
30. Lee C, Kim CS (2013) Contrast enhancement based on layered difference representation. Proceedings of the IEEE international conference on image processing (ICIP) 22(12):5372–5384
31. Lee C, Kim CS (2013) Contrast enhancement based on layered difference representation of 2d histograms. IEEE Trans Image Process 22:5372–5384
32. Lee CH, Shih JL, Lien C, Han CC (2013) Adaptive multiscale retinex for image contrast enhancement. In: 2013 International conference on signal-image technology internet-based systems, pp 43–50
33. Li C, Guo C, Chen CL (2021) Learning to enhance low-light image via zero-reference deep curve estimation. IEEE Trans Pattern Anal Mach Intell, pp 1–1. https://doi.org/10.1109/TPAMI.2021.3063604
34. Li M, Liu J, Yang W, Sun X, Guo Z (2018) Structure-revealing low-light image enhancement via robust retinex model. IEEE Trans Image Process 27:2828–2841
35. Liang J, Zhang X (2015) Retinex by higher order total variation $l_1$ decomposition. J Math Imaging Vis 52:345–355
36. Liu YF, Guo JM, Lai BS, Lee JD (2013) High efficient contrast enhancement using parametric approximation. In: 2013 IEEE International conference on acoustics, speech and signal processing, pp 2444–2448
37. Liu YF, Guo JM, Yu JC (2016) Contrast enhancement using stratified parametric-oriented histogram equalization. IEEE Trans Circuits Syst Video Technol 27(6):1171–1181
38. Liu B, Jin W, Chen Y, Liu C, Li L (2011) Contrast enhancement using non-overlapped sub-blocks and local histogram projection. IEEE Trans Consum Electron 57(2):583–588
39. Liu J, Xu D, Yang W, Fan M, Huang H (2021) Benchmarking low-light image enhancement and beyond. Int J Comput Vis 129:1153–1184
40. Lore KG, Akintayo A, Sarkar S (2017) Llnet: a deep autoencoder approach to natural low-light image enhancement. Pattern Recogn 61:650–662
41. Ma K, Duanmu Z, Yeganeh H, Wang Z (2018) Multi-exposure image fusion by optimizing a structural similarity index. IEEE Trans Computat Imaging 4:60–72
42. Mittal A, Soundararajan R, Bovik A (2013) Making a "completely blind" image quality analyzer. IEEE Signal Process Lett 20:209–212
43. Ng M, Wang W (2011) A total variation model for retinex. SIAM J Imaging Sci 4:345–365
44. Pang J, Zhang S, Bai W (2017) A novel framework for enhancement of the low lighting video. In: 2017 IEEE Symposium on computers and communications (ISCC), pp 1366–1371. https://doi.org/10.1109/ISCC.2017.8024714
45. Pizer S, Johnston R, Ericksen JP, Yankaskas B, Muller K (1990) Contrast-limited adaptive histogram equalization: speed and effectiveness. In: [1990] Proceedings of the first conference on visualization in biomedical computing, pp 337–345

46. Provenzi E, Carli LD, Rizzi A, Marini D (2005) Mathematical definition and analysis of the retinex algorithm. J Optic Soc Am. A, Optics, image science, and vision 22(12):2613–21
47. Rahman Z, Aamir M, fei Pu Y, Ullah F, Dai Q (2018) A smart system for low-light image enhancement with color constancy and detail manipulation in complex light environments. Symmetry 10:718
48. Rahman Z, Jobson DJ, Woodell GA (2004) Retinex processing for automatic image enhancement. J Electronic Imaging 13:100–110
49. Ren X, Yang W, Cheng WH, Liu J (2020) Lr3m: Robust low-light enhancement via low-rank regularized retinex model. IEEE Trans Image Process 29:5862–5876
50. Shan Q, Jia J, Brown MS (2010) Globally optimized linear windowed tone mapping. IEEE Trans Vis Comput Graph 16:663–675
51. Singh RP, Dixit M (2015) Histogram equalization: a strong technique for image enhancement. International Journal of Signal Processing. Image Process Pattern Recognit 8(8):345–352
52. Singh K, Kapoor R (2014) Image enhancement using exposure based sub image histogram equalization. Pattern Recogn Lett 36:10–14
53. Tao L, Zhu C, Xiang G, Li Y, Jia H, Xie X (2017) Llcnn: a convolutional neural network for low-light image enhancement. In: 2017 IEEE Visual communications and image processing (VCIP), pp 1–4
54. Wang Y, Chen Q, Zhang B (1999) Image enhancement based on equal area dualistic sub-image histogram equalization method. IEEE Trans Consumer Electron 45(1):68–75
55. Wang Y, Yin W, Zeng J (2019) Global convergence of admm in nonconvex nonsmooth optimization. J Sci Comput 78:29–63
56. Wang S, Zheng J, Hu HM, Li B (2013) Naturalness preserved enhancement algorithm for non-uniform illumination images. IEEE Trans Image Process 22:3538–3548
57. Wei C, Wang W, Yang W, Liu J (2018) Deep retinex decomposition for low-light enhancement. In: BMVC
58. Wu Y, Song W, Zheng J, Liu F (2020) Noisy low-light image enhancement using reflectance similarity prior. In: 2020 15th IEEE international conference on signal processing (ICSP), vol 1, pp 160–164. https://doi.org/10.1109/ICSP48669.2020.9321010
59. Xu L, Yan Q, Xia Y, Jia J (2012) Structure extraction from texture via relative total variation. ACM Transactions on Graphics (TOG) 31:1–10
60. Xu Y, Yin W, Wen Z, Zhang Y (2011) An alternating direction algorithm for matrix completion with nonnegative factors. Frontiers Math China 7:365–384
61. Xu J, Yu M, Liu L, Zhu F, Shao L (2020) Star: a structure and texture aware retinex model. IEEE Trans Image Process 29:5022–5037
62. Yan J, Lin S, Kang SB, Tang X (2014) A learning-to-rank approach for image color enhancement. In: 2014 IEEE Conference on computer vision and pattern recognition, pp 2987–2994
63. Ying Z, Li G, Gao W (2017) A bio-inspired multi-exposure fusion framework for low-light image enhancement. arXiv:1711.00591
64. Yu R, Liu W, Zhang Y, Qu Z, Zhao D, Zhang B (2018) Deepexposure: Learning to expose photos with asynchronously reinforced adversarial learning. In: NeurIPS
65. Yuan LT, Swee SK, Ping TC (2015) Infrared image enhancement using adaptive trilateral contrast enhancement. Pattern Recogn Lett 54:103–108
66. Zhang Y, Guo X, Ma J, Liu W, Zhang J (2021) Beyond brightening low-light images. Int J Comput Vis 129(4):1013–1037
67. Zhang Y, Zhang J, Guo X (2019) Kindling the darkness: a practical low-light image enhancer. In: Proceedings of the 27th ACM International conference on multimedia
68. Zhao Z, Xiong B, Wang L, Ou Q, Yu L, Kuang F (2022) Retinexdip: a unified deep framework for low-light image enhancement. IEEE Trans Circuits Syst Video Technol 32:1076–1088
69. Zheng S, Gupta G (2022) Semantic-guided zero-shot learning for low-light image/video enhancement. In: Proceedings of the IEEE/CVF Winter conference on applications of computer vision, pp 581–590
70. Çelik T., Tjahjadi T (2011) Contextual and variational contrast enhancement. IEEE Trans Image Process 20:3431–3441

**Xuesong Li** is pursuing his MS degree at the School of Electrical and Electronic Engineering, Shandong University of Technology, Zibo, China. His research interests include image processing and pattern recognition.

**Qilei Li** is currently a PhD student with the School of Electronic Engineering and Computer Science, Queen Mary University of London, London, United Kingdom. He received the M.S. degree in signal and information processing from Sichuan University. His research interests are computer vision and deep learning.

**Marco Anisetti** is an Associate Professor at the Università degli Studi di Milano, Italy. He received the Ph.D degree in Computer Science from the Università degli Studi di Milano in 2009. He is the winner of the GIRPR award for the best PhD thesis in 2010 and the winner of Chester Sall Award from IEEE Consumer Electronics Society in 2009. His research interests are in the area of Computational Intelligence and its application to the design and evaluation of complex systems and services.

**Gwanggil Jeon** received the B.S., M.S., and Ph.D. (summa cum laude) degrees from the Department of Electronics and Computer Engineering, Hanyang University, Seoul, Korea, in 2003, 2005, and 2008, respectively. He is currently an IEEE Senior Member and a Full Professor at Incheon National University, Incheon, Korea. His research includes Signal and Image Processing, IoT, Healthcare, Sustainable Cities and Society, Embedded System, etc.

**Mingliang Gao** received his Ph.D. in communication and information systems from Sichuan University, Chengdu, China, in 2013. He is currently an associate professor at the School of Electrical and Electronic Engineering, Shandong University of Technology, Zibo, China. His main research interests include computer vision and deep learning.